Silicon Micromachined Ultrasonic Transducers

B. T. Khuri-Yakub, F. L. Degertekin, X-C. Jin, S. Calmes, I. Ladabaum, S. Hansen, and X. J. Zhang

E. L. Ginzton Laboratory
Stanford University
Stanford, CA 94305-4085

Abstract This paper reviews ultrasonic transducers that are made by silicon micromachining (MUTs). Transducers for both air-borne and immersion applications are made from parallel plate capacitors whose dimensions are controlled through traditional integrated circuit manufacturing methods. Typical dimensions of the capacitors are: gap < 1 micron (vacuum or air), membrane thickness = 1 micron (silicon nitride or poly-silicon), and diameter = 50 microns. A large number of small elements are connected in parallel to make a transducer. Transducers for air borne ultrasound applications have been operated in the frequency range of 0.1-11 MHz, while immersion transducers have been operated in the frequency range of 1-20 MHz.

A theoretical model for the transducers will be presented. The model is used to highlight the important parameters in the design of both airborne and immersion transducers. Theory is used to compare the receive sensitivity, the transmit power capability, and the bandwidth of the MUTs to piezoelectric transducers. We will show that MUTs are at least as good if not better performing than piezoelectric transducers. Examples of single element transducers, linear array transducers, and two dimensional arrays of transducers will be presented. The agreement between the theory and experimental measurements will be presented and will prove the validity of the model.

In summary, we will present a capacitive micromachined transducer technology that is competitive to the piezoelectric technology and that carries the advantage of electronic integration and batch processing using silicon fabrication practices.

INTRODUCTION

Capacitors have been used as ultrasound transducers for quite some time[1]. Traditional designs had relatively large gaps, 50-100 μm, and used the air in the gap as the restoring force of the vibrating electrode. These transducers suffered from low efficiency. We propose a design where silicon micromachining is used to define the capacitors. In this implementation, the gaps are made as small as 500Å, and the restoring force of the vibrating electrode is the stiffness of the electrode itself. This approach makes possible very efficient transducers, indeed, it makes possible transducers that are competitive with piezoelectric transducers in terms of efficiency and bandwidth[2,3]. One advantage of these transducers is the ability to integrate electronics on the same silicon wafer where the transducers are made. Another is the potential for making one-dimensional, and two-dimensional, and annular arrays of transducers using simple photolithography.

THEORY AND MODEL

We use Mason's model to represent the capacitor transducer [4]. A schematic of the transducer and its equivalent circuit are shown in Fig.1.

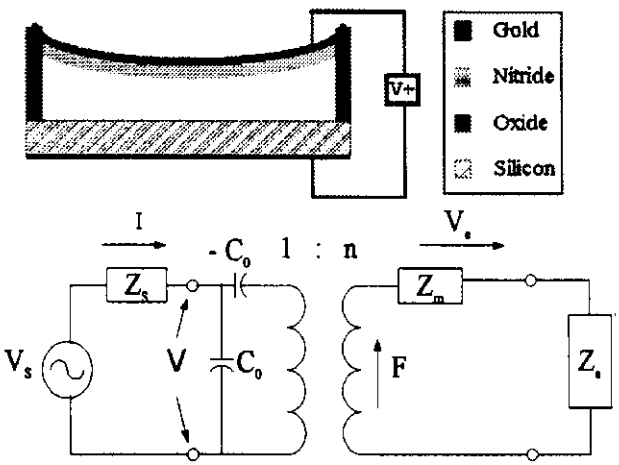

Fig.1 Schematic of a capacitor transducer and its equivalent circuit.

A metal coated silicon nitride membrane is used as the vibrating membrane electrode of the capacitor. Standard integrated manufacturing processes are used to define the dimensions of the capacitor. Residual stress in the membrane is controlled via the process of chemical vapor deposition and is held at a few hundred MPas [5].

In the equivalent circuit, C_0 is the capacitance of the device, Z_t is the impedance of the source, Z_m is the impedance of the medium (air or

0-7803-4095-7/98/$10.00 © 1998 IEEE

water), Z_m is the mechanical impedance of the membrane given by:

$$Z_m = j\omega\rho l_t\left[\frac{ak_1k_2\left(k_2J_0(k_1a)J_1(k_2a)+k_1J_1(k_1a)J_0(k_2a)\right)}{ak_1k_2\left(k_2J_0(k_1a)J_1(k_2a)+k_1J_1(k_1a)J_0(k_2a)\right)-2\left(k_1^2+k_2^2\right)J_1(k_1a)J_1(k_2a)}\right]$$

where ω is the radian frequency, ρ is the density of the membrane, l_t is the thickness of the membrane, J_0 and J_1 are zeroth and first order o Bessel functions of the first kind, and k_1 and k_2 are given by:

$$k_1 = \sqrt{\frac{\sqrt{d^2+4c\omega^2}-d}{2c}}$$

And

$$k_2 = \sqrt{\frac{\sqrt{d^2+4c\omega^2}+d}{2c}}$$

Where:

$$c = \frac{(Y_0+T)l_t^2}{12\left(1-\sigma^2\right)}$$

And

$$d = \frac{T}{\rho}$$

where Y_0 is Young's modulus, T is the residual stress, and σ is the Poisson's ratio all of the membrane material.

The impedance of the membrane can be represented by a series RLC circuit with a resistance corresponding to the attenuation of the membrane.

The transformer ratio in the equivalent circuit allows the transformation between the mechanical and electrical ports of the device. It is given by:

$$n = V_{dc}\frac{\varepsilon_0\varepsilon^2 S}{\left(\varepsilon_0 l_t+\varepsilon l_a\right)^2}$$

where V_{dc} is the dc bias on the electrode, ε_0 is the dielectric constant of free space, ε is the dielectric constant of the membrane material, S is the area of the transducer, and l_a is the thickness of the air gap. In short, the transformer ratio is equal to the dc electric field multiplied by the unbiased capacitance of the transducer.

The importance of the approach we propose lies in the fact that the transformer ratio can be made very large. The capacitance of the capacitor can be 10s of Farads, and the electric field can be as high at 10^8 V/m. The high electric field is reached because the gap of the capacitor can be made as small as 500Å. It is easy to see why the sensitivity of these capacitors is so much higher than earlier designs. The gap being several orders of magnitude smaller implies a relative change in capacitance that is the same number of orders of magnitude higher!

In a typical capacitor, a membrane is in the range of 20-100 microns in diameter. Thus, to make a transducer, a very large number of membranes are electrically connected in parallel using a lithography step. This use of lithography allows the manufacture of single elements, or array elements side by side on the same wafer and in one step.

In an air transducer, the impedance of the membrane at resonance is comparable in value to the impedance of air. Thus, the transducer has a characteristic resonant behavior shown in Fig. 2.

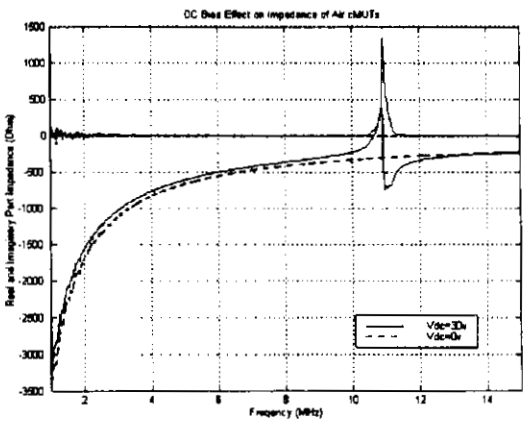

Fig. 2 Input impedance of air cMUT.

The transducer of Fig. 2 shows that without dc bias the real part of the input impedance is zero and the imaginary part is just a capacitor. As the dc bias is applied, and resonant peak representing real power coupled into the sound wave is seen to exist at the resonant frequency of the transducer. It is important to recognize that the impedance shown is the measured impedance of a capacitor transducer!

In immersion applications, the impedance of the membrane is smaller than the impedance of water and can be ignored in comparison. Thus, the input impedance of an immersion transducer has no resonance and consists only of a series (or parallel) RC circuit [6]. Thus, impedance matching the electronics to the RC circuit determines the bandwidth and efficiency of the transducer.

The performance of the cMUT and the piezoelectric transducer are evaluated to establish the relative merits of both types of transducers. For a vehicle for the comparison, a square element 400 microns on the side is used. This size of transducer is used because it constitutes an element in a two-dimensional array needed for an underwater camera. The design calls for a center frequency of operation

of 3 MHz with a bandwidth enabling operation at 0.75 MHz. To compare the two types of transducers, the KLM model is used to represent the piezoelectric transducer, and the Mason model outlined above is used to represent the capacitive transducer.

We use PZT 5H for the piezoelectric, and we assume a perfect match into water using one matching layer. The cMUT has an air gap of 1500 Å, a nitride membrane thickness of 8000 Å, a cell radius of 18 μm, and operating at a dc voltage of 100 Volts.

The performance of each device as a transmitter is determined by calculating the pressure at the face of the transducer that is generated by applying 1 volt at its input terminals. The receive sensitivity is calculated by evaluating the receiver voltage due to an input pressure of 1 Pa at the face of the transducer. This output voltage is calculated assuming an amplifier with an input resistance of 300 kΩ and capacitance of 0.1 pF. The noise due to the real part of the input impedance of the transducer is also calculated in order to determine the total signal--to-noise ratio of the receiver. This signal to noise is calculated per volt and per square root Hz. Finally, the total dynamic range of the system is calculated by adding together the transmitter and the receiver sensitivities for each transducer. Figure 4 shows the result of this comparison:

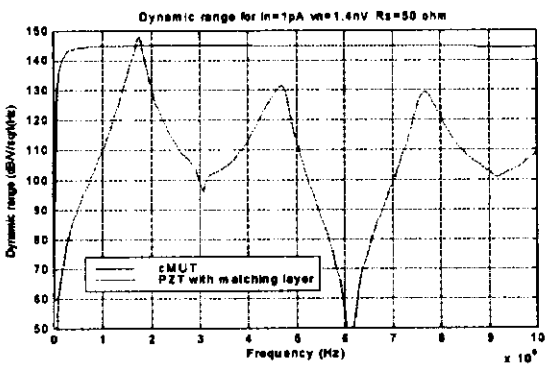

Fig. 4 Comparison of the dynamic ranges of a cMUT and a piezoelectric transducer.

The above comparison shows that the cMUT can have as good a dynamic range as a piezoelectric transducer and a much larger bandwidth. Indeed, for an underwater camera, the cMUT is a far superior device as it permits operation at both 0.75 MHz and 3.0 MHz. It is important to note that for this transducer, the high frequency limit is 50 MHz. The minimum insertion loss and bandwidth are determined by electrical matching considerations of the transducer to the electronic circuit. For other immersion applications such as medical imaging and non-destructive evaluation, the same benefits hold. Similar arguments and calculations can be made for one dimension array elements and single element transducers. When the area of a cMUT becomes large and the capacitance decreases, it becomes more and more difficult to match the transducer into electronics and thus a practical limit is set on the size of transducers that can be realistically developed using this technology.

TRANSDUCER FABRICATION

Standard integrated circuit fabrication processes are used to make the capacitive transducers. Figure 5 shows the process presently used for making transducers.

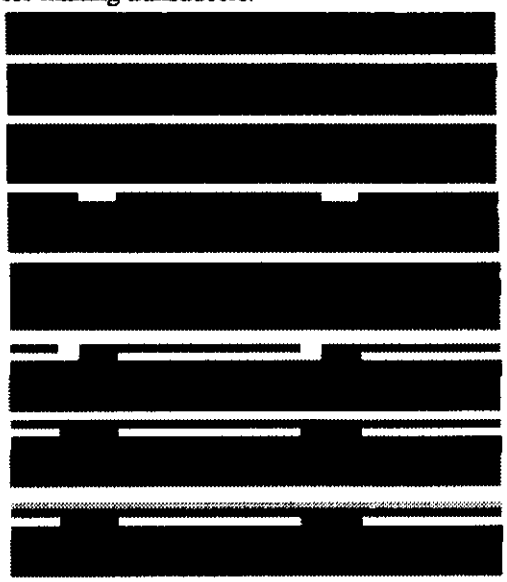

Fig. 5 Schematic of the processing schedule used for making cMUTs.

First, the silicon wafer receives a high doping density ion implantation to form the back contact of the capacitor. Then, a layer of insulating silicon nitride is deposited to protect the back contact and as an etch stop. An amorphous silicon sacrificial layer is deposited over the wafer. The sacrificial layer is defined by photolithography. The amorphous silicon is left in regions that will become vacuum gaps. Another silicon nitride layer is deposited over the amorphous silicon. Holes are defined at the edges of the amorphous silicon which is then removed by wet etching. Silicon nitride is again deposited and used to plug the holes through which the etching fluid was introduced. Finally, a gold layer is deposited over the wafer to define the top electrode of the capacitor. A scanning electron microscope image of a finished device is shown in Fig. 6.

The individual cells are connected electrically in parallel using the gold metal. The

metal over each cell is clearly seen to be one half the diameter of each cell. The size of the electrode is reduced to reduce the capacitance of the device without reducing the displacement at the surface of the membrane.

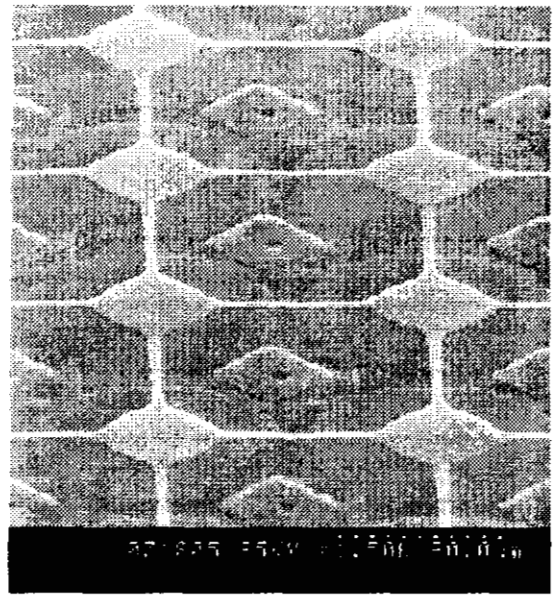

Fig. 6 SEM of a finished cMUT.

EXPERIMENTAL RESULTS

Immersion and air transducers are evaluated via measurements of their electrical input impedance, input response and bandwidth, beam profile and insertion loss. Figure 7 shows a measurement of the input impedance of an immersion transducer and its comparison to theory.

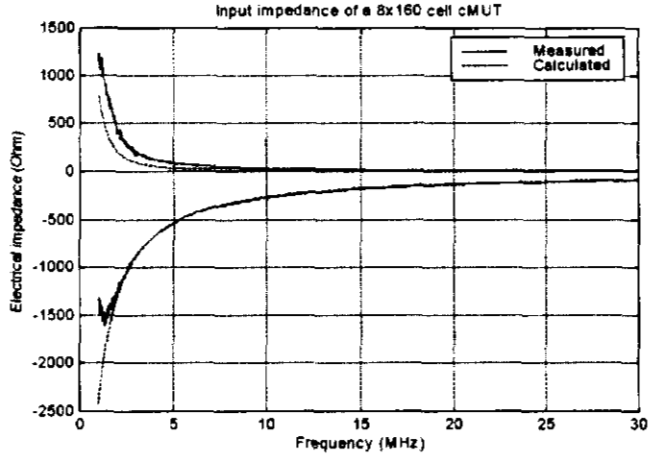

Fig. 7 Comparison of the theoretical and measured input impedance of an immersion transducer.

Figure 7 shows that immersion transducers can be made according to design. There is an excellent fit between theory and experiment. However, in order to fit the theory, the impedance of the medium, in this case water, has to be increased in order to fit the experiment. In other words, an extra loss term has to be added to account for the insertion loss of the transducer. Initial measurements and theoretical calculations indicate that energy is coupled to the silicon bulk or wafer in the form of Lamb waves. Another paper at this symposium will detail these measurements and calculations [7].

The impulse response of an immersion transducer is shown in Fig. 8.

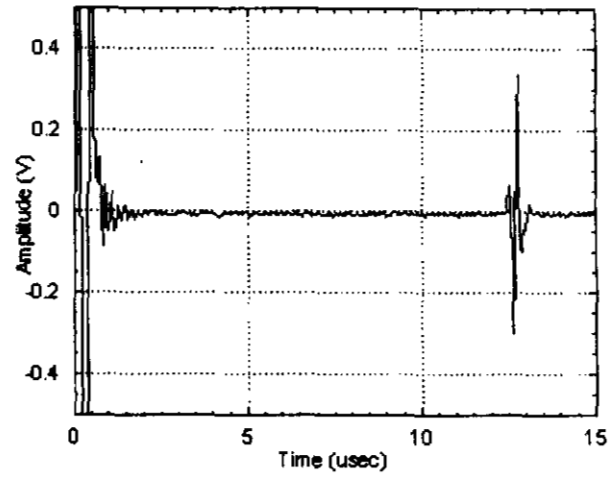

Fig. 8 Impulse response of an immersion transducer.

The impulse response of the transducer shows the large bandwidth that is characteristic of capacitive ultrasonic transducers. The measured fractional bandwidth is over 100%, which is limited by the electronics and not the transducer.

A measurement of the insertion loss of the device shows that there is a one way loss of 5dB which is due to coupling into the propagation modes of the wafer.

Air transducers have a similar performance to the immersion transducers. The main difference is in the bandwidth being much less and of the order of 5%. This small bandwidth is a result of the device performance being dominated by the resonance of the membrane. Figure 9 shows the impulse response of an air transmission experiment. Two identical transducers are used to transmit and receive a 2.3 MHz pulse after propagation through an aluminum sample. The transmitter transducer is excited with a 20 cycles tone burst. The rise time and fall time of the received pulse is a measure of the bandwidth of the transducer, which is about 5%. Transmission through aluminum indicates that the transmission system has over 100 dB dynamic range. Thus, non-

destructive evaluation is enabled using micro machined ultrasonic air transducers.

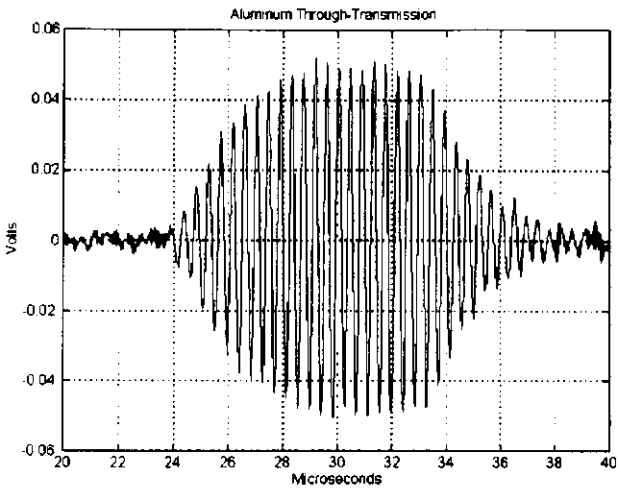

Fig. 9 Air borne ultrasound pulse transmission through an aluminum sample.

The air transducers have a one way insertion loss of 10 dB. This loss is due to coupling of a Lamb wave into the structure [8].

ARRAYS

One of the main features of the cMUT technology is the ability to use photolithography to define the transducer. Arrays, one dimension or two dimension, can thus be formed in one step. The same wafer can be used to make single or multiple element transducers. Another feature of the cMUT is that the transducer thickness is that of the silicon wafer. A 20 cm wafer has a thickness of 0.75 mm, whereas a 10 cm wafer is about 0.5 mm thick. Thus, the profile of an array can be very thin.

Electronic circuits can be integrated on the same wafer as the transducers. Or, the transducer wafer can be flip chip bonded to an electronics wafer without much increase in the profile of the array.

Figure 10 shows the picture of a 64 elements 1-D array.

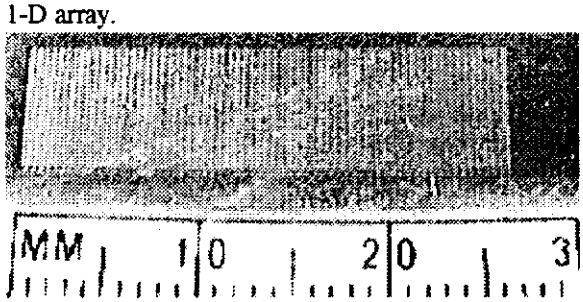

Fig. 10 Picture of a 1-D array

The elements of the 1-D array are on 0.4 mm centers and have a length of 5.6 mm. Each element consists of a number of drums that are connected in parallel in the same fashion as the single element transducers. Figure 11 shows the details of an array element.

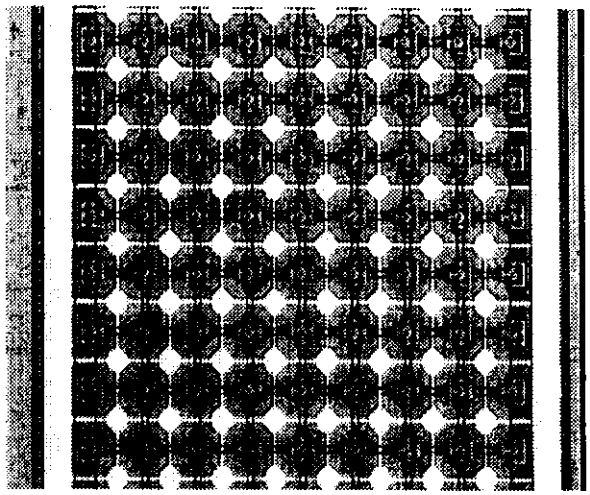

Fig. 11 Picture of individual drum heads making on 1-D element.

The 64 elements 1-D array was used to image a 0.4mm x 0.4mm element which is considered a point source. Simple time delay reconstruction of the raw rf data was done. The result of this reconstruction is shown in Fig. 12.

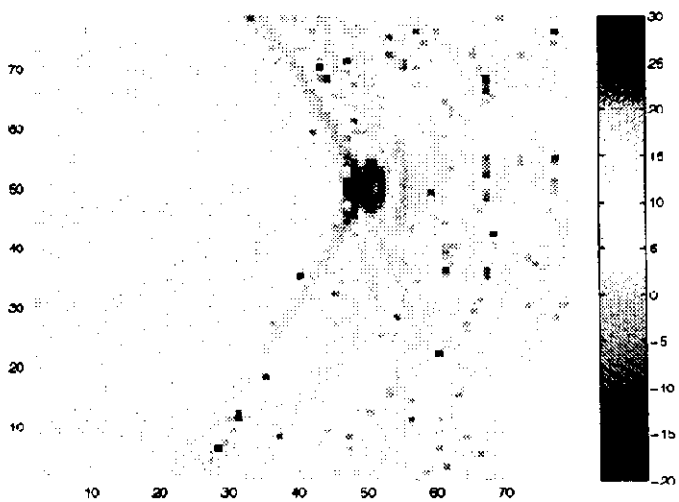

Fig. 12 Reconstructed image of a 0.4mm x 0.4mm point source.

The elements of the 1-D array excited Lamb waves in the silicon wafer. This energy leaks back into the fluid and introduces a null in the acceptance angle of the array element. A typical beam profile of

a single element is shown in Fig. 13. Again, a more detailed discussion of lateral coupling is presented at another presentation at this same symposium [7].

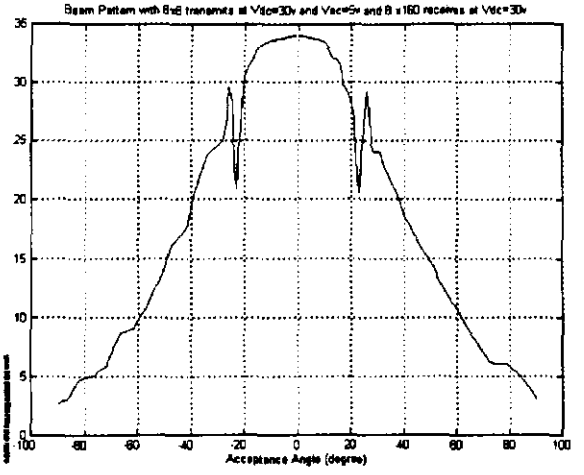

Fig. 13 Acceptance angle of an element of the 1-D array at a frequency of 4 MHz.

This problem with the beam profile of an array element can be reduced by thinning the wafer or by adding porous silicon or trenches between the array elements.

Two dimension arrays are as easy to make as the 1-D arrays. Figure 14 shows a 5 by 5 2-D array made in the same processing run as the single elements and 1-D arrays presented earlier.

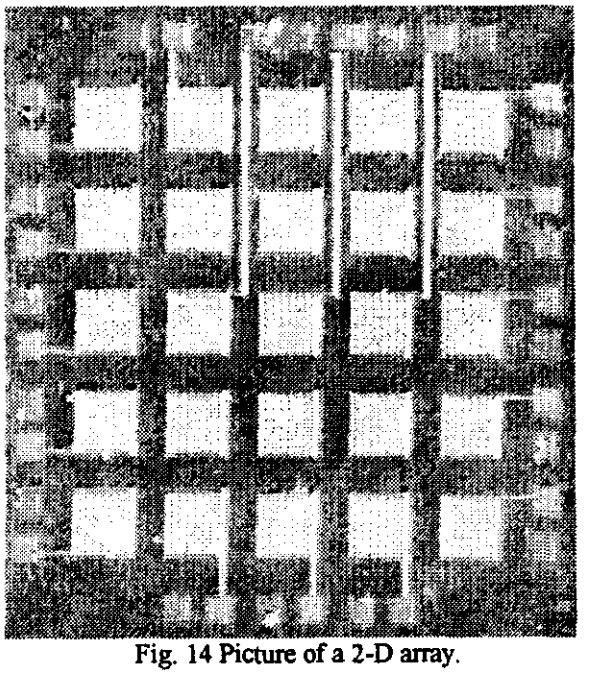

Fig. 14 Picture of a 2-D array.

Again, each element of the 2-D array is made by connecting in parallel a number of individual drum heads.

The cross coupling between elements and the beam profiles of the 2-D array elements are in excellent agreement with theoretical predictions. The problem of coupling into a Lamb wave is quite reduced. The reduction in cross coupling is due to the fact the each element acts as a point source transmitter and receiver which reduces the coupling problem. Figure 15 shows the beam profile of a 2-D array element at frequency of 4 MHz.

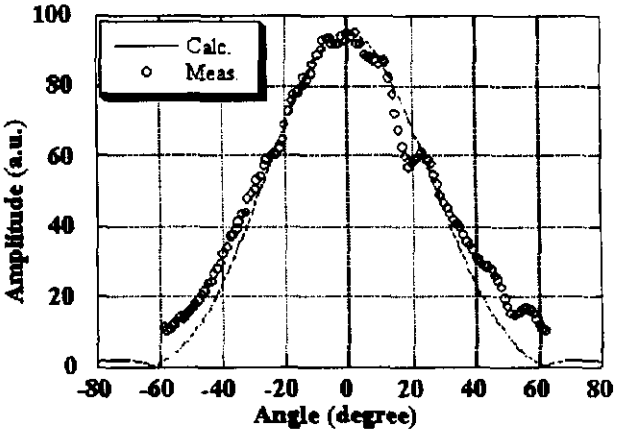

Fig. 15 Acceptance angle of an element of the 2-D array at a frequency of 4 MHz.

There is a slight ripple in the acceptance angle at 12° and 22° where the lowest order antisymmetric and symmetric Lamb waves are excited at 4 MHz in a 0.5 mm thick silicon wafer. This problem is small and can be further reduced as mentioned earlier.

CONCLUSIONS

Silicon micromachining can be used to make capacitive ultrasonic transducers that are competitive with piezoelectric transducers in terms of efficiency and bandwidth. They offer the promise of ease of manufacture in 1-D and 2-D arrays and of integration with electronic circuitry.

ACKNOWLEDGEMENTS

This research was supported by DARPA, ONR, and AFOSR.

REFERENCES

1. W. Khul, G.R. Schodder and F.K. Schodder, "Condenser transmitters and microphones with solid dielectric for airborne ultrasonics," *Acoustica*, vol. 4, pp. 520-32, 1954.
2. M.I. Haller and B.T. Khuri-Yakub, "A surface micromachined electrostatic ultrasonic air transducer," *IEEE Trans. on UFFC*, vol. 43, no.1, pp. 1-6, 1996.
3. I. Ladabaum, T. Soh, X.C. Jin, A. Atalar and B.T. Khuri-Yakub, "Micromachined ultrasonic transducers," *IEEE Trans. on UFFC*, vol. 45, pp. 678-90, 1998.
4. W. P. Mason, *Electromechanical Transducers and Wave Filters*, 2nd edition, 1948.
5. X.C. Jin, I. Ladabaum and B.T. Khuri-Yakub, "The microfabrication of capacitive ultrasonic transducers," *IEEE/ASME J. Micro-electro-mechanical Systems*, vol.7, no.3, pp.295-302, 1998.
6. X.C. Jin, I. Ladabaum and B.T. Khuri-Yakub, "Surface micromachined capacitive ultrasonic immersion transducers," *Proceedings of IEEE Workshop on Microelectromechanical Systems*, pp. 649-54, 1998.
7. X.C. Jin, F.L. Degertekin, S. Calmes, X.J. Zhang, I. Ladabaum and B.T. Khuri-Yakub, "Micromachined capacitive transducer arrays for medical ultrasound imaging," *Proceedings of IEEE Ultrasonic Symposium*, 1998.
8. A. Bozkurt, F.L. Degertekin, A. Atalar, B.T. Khuri-Yakub, "Analytic modeling of loss and cross-coupling in capacitive micromachined ultrasonic transducers," *Proceedings of IEEE Ultrasonic Symposium*, 1998.